

# Effect of cationic nonstoichiometry on thermoelectric properties of layered calcium cobaltite obtained by field assisted sintering technology (FAST)

Andrei I. Klyndyuk<sup>a,\*</sup>, Dzmitry S. Kharytonau<sup>b,\*\*</sup>, Iryna V. Matsukevich<sup>c</sup>, Ekaterina A. Chizhova<sup>a</sup>, Zoltán Lenčič<sup>d</sup>, Robert P. Socha<sup>b,e</sup>, Małgorzata Zimowska<sup>b</sup>, Ondrej Hanzel<sup>d</sup>, Marián Janek<sup>f</sup>

<sup>a</sup> Belarusian State Technological University, 220006, Minsk, Belarus

<sup>b</sup> Jerzy Haber Institute of Catalysis and Surface Chemistry, Polish Academy of Sciences, 30 239, Krakow, Poland

<sup>c</sup> FunGlass – Center for Functional and Surface Functionalized Glass, Alexander Dubček University of Trenčín, 911 50, Trenčín, Slovakia

<sup>d</sup> Institute of Inorganic Chemistry, Slovak Academy of Sciences, 845 36, Bratislava, Slovakia

<sup>e</sup> CBRTTP Research and Development Center of Technology for Industry, 00 645, Warsaw, Poland

<sup>f</sup> Slovak University of Technology in Bratislava, 812 37, Bratislava, Slovakia

## ARTICLE INFO

Handling Editor: P. Vincenzini

### Keywords:

Hot pressing

Composites

Electrical properties

Thermal properties

## ABSTRACT

This work addresses the problem of obtaining of  $\text{Ca}_3\text{Co}_4\text{O}_{9+\delta}$ -based ceramics with enhanced thermoelectric performance. Phase-inhomogeneous layered calcium cobaltite ceramics with cationic nonstoichiometry were prepared by solid-state reactions method and a field assisted sintering technology (FAST). Comprehensive experimental characterizations were conducted on the prepared bulk samples, focusing on their phase composition, as well as thermal (including thermal expansion, thermal diffusivity, and thermal conductivity), electrical (encompassing electrical conductivity and the Seebeck coefficient), and functional properties (such as power factor and figure-of-merit). The FAST technique allowed to obtain ceramics with low porosity and high electrical conductivity, which increased as the Ca:Co ratio within the samples decreased, while sample phase inhomogeneity considerably increased the Seebeck coefficient. The best thermoelectric performance was demonstrated for cationic nonstoichiometric  $\text{Ca}_3\text{Co}_{4.4}\text{O}_{9+\delta}$ , which power factor and figure-of-merit values at 825 °C reached  $427 \mu\text{W}\cdot\text{m}^{-1}\cdot\text{K}^{-2}$  and 0.146, respectively.

## 1. Introduction

Nowadays, about two-thirds of all energy used is being lost as waste heat, and the growing energy crisis underlines a compelling need for high-performance energy conversion strategies [1]. Thermoelectric generators (TEGs) are solid-state devices that can directly and effectively convert heat evolving into the environment by industrial enterprises, transport vehicles, and engines to electric energy. The production of TEG requires materials that can statically interconvert thermal and electrical energy using the motion of solid internal carriers [1,2]. Such materials should possess high values of electrical conductivity ( $\sigma$ ) and the Seebeck coefficient ( $S$ ), and low thermal conductivity ( $\lambda$ ) [3]. Typical thermoelectrics are chalcogenides of Bi, Sb, Sn, and their solid solutions, which have high values of power factor ( $PF$ ) and thermoelectric figure-of-merit ( $ZT$ ). Such substances have been widely used in

various thermoelectric devices since the 2<sup>nd</sup> half of the 20<sup>th</sup> century. These materials, have a number of drawbacks, such as high content of toxic and expensive components (such as Bi, Sb, Te, Se, etc.) and low oxidation stability by atmospheric oxygen at high operation temperatures [3,4].

Recently, a novel type of oxide thermoelectrics based on layered cobaltites ( $\text{Na}_x\text{CoO}_2$ ,  $\text{Ca}_3\text{Co}_4\text{O}_{9+\delta}$ ,  $\text{Bi}_2\text{Ca}_2\text{Co}_{1.7}\text{O}_y$ , etc.) has been extensively examined as promising candidates for the development of  $p$ -branches of TEGs operating at high temperatures [4,5]. These materials overcome the limitations of traditional bismuth-based thermoelectrics and can operate at high temperatures without special protective atmospheres [6]. Layered calcium cobaltite ( $\text{Ca}_3\text{Co}_4\text{O}_{9+\delta}$ ) has a monoclinic structure, which is formed by alternating  $[\text{Ca}_2\text{CoO}_3]$  (rock salt (NaCl) structure) and  $[\text{CoO}_2]$  ( $\text{CdI}_2$  structure) structural units. These layers have different periodicity in one direction, so this compound belongs to

\* Corresponding author.

\*\* Corresponding author.

E-mail addresses: [klyndyuk@belstu.by](mailto:klyndyuk@belstu.by) (A.I. Klyndyuk), [dmitry.kharitonov@ikif.edu.pl](mailto:dmitry.kharitonov@ikif.edu.pl) (D.S. Kharytonau).

<https://doi.org/10.1016/j.ceramint.2024.05.402>

Received 8 April 2024; Received in revised form 22 May 2024; Accepted 24 May 2024

Available online 24 May 2024

0272-8842/© 2024 Elsevier Ltd and Techna Group S.r.l. All rights are reserved, including those for text and data mining, AI training, and similar technologies.

the so-called “misfit-layered phases” [7]. The practical usage of  $\text{Ca}_3\text{Co}_4\text{O}_{9+\delta}$ -based ceramics synthesized using the precursor powder mixing as a traditional ceramic synthesis method is limited due to its high porosity, low mechanical strength, and electrical conductivity [8].

The thermoelectric (functional) properties of ceramics based on the layered calcium cobaltite can be improved by using low-temperature “solution” synthesis methods [9–11] or self-propagating high-temperature synthesis [12] instead of the traditional ceramic method. To improve their performance, special sintering methods, such as hot-pressing (HP) [8,9,13,14], spark plasma sintering (SPS) [10,11,14–18], oscillatory pressure sintering (OPS) [19] or so-called two-step sintering (TSS) (pressure-less sintering/annealing method) [20–23] can be applied instead of conventional sintering (CS). It has been shown by different authors [8,11,18,21,23,24], that such sintering results in lower porosity of ceramics and, as a consequence, in the increase of its  $\sigma$  values.

Other ways to improve the functional properties of  $\text{Ca}_3\text{Co}_4\text{O}_{9+\delta}$  are a partial substitution of calcium in its crystal structure by rare-earth elements [25,26], bismuth [27–29] or copper [30] or of cobalt by heavy and transition metals [28,31–35], nanostructuring [36,37], and creation of chemical [38] or phase inhomogeneity in ceramics [2,18,22,23,39–51]. According to our previous studies [22,23,29,45] and literature data [2,40,47,49–51], phase-inhomogeneous ceramics demonstrated larger values of  $S$  than the single phase one.

The phase inhomogeneity in layered calcium cobaltite can be introduced by adding the second (e.g. as impurity) phase at the synthesis or the sintering stage. Such approach was successfully verified in works [39–44,46–48,50,51], where the authors studied the effect of the addition of micro- and nanoparticles of Ag [39–41], single and double metal oxides [42–44,49], or carbides [2,46,47,50] on the microstructure, electrical transport, and functional properties of composite ceramics.

According to Ref. [52], layered calcium cobaltite in air may exist in the range of continuous compositions  $\text{Ca}_3\text{Co}_{3.87}\text{O}_{9+\delta}$ – $\text{Ca}_3\text{Co}_{4.07}\text{O}_{9+\delta}$ . To create the multiphase layered cobaltite systems, the introduction of the cationic nonstoichiometry in the samples to obtain the target composition beyond the  $\text{Ca}_3\text{Co}_4\text{O}_{9+\delta}$  homogeneity area (so-called self-doping) was verified [18,22,48,49]. To the best of our knowledge, the effect of self-doping for the creation of cationic nonstoichiometry combined with HP for improvement of the electrical conductivity on the overall thermoelectric performance of  $\text{Ca}_3\text{Co}_4\text{O}_{9+\delta}$ -based thermoelectric materials were not widely examined in the literature. It was shown in our previous publication [53], that hot-pressing allows to obtain ceramics with low porosity and large electrical conductivity values. At the same time, the Seebeck coefficient of ceramics increased due to the creation of phase inhomogeneities. These effects opened up the possibility to obtain thermoelectric material with improved thermoelectric characteristics compared to those of materials produced by traditional ceramic synthesis method. The complex study of such materials using a number of independent methods would be very interesting but it has not been performed yet.

The aim of this work was to synthesize and investigate  $\text{Ca}_3\text{Co}_4\text{O}_{9+\delta}$ -based ceramics with cationic nonstoichiometry obtained by a field assisted sintering technology (FAST), also called rapid hot-pressing. The materials obtained were characterized by X-ray diffraction (XRD), scanning electron microscopy combined with energy-dispersive X-ray spectroscopy (SEM/EDX), Fourier-transform infrared spectroscopy (FTIR), and X-ray photoelectron spectroscopy (XPS). The ceramics thermal properties, such as thermal expansion, thermal diffusivity, and  $\lambda$  were examined within a temperature range from 25 °C to 825 °C. In addition, the anisotropy of electrical and functional (thermoelectric) properties of obtained materials was investigated.

## 2. Experimental

Powders with the final composition of  $\text{Ca}_3\text{Co}_{3.6}\text{O}_{9+\delta}$ ,  $\text{Ca}_3\text{Co}_4\text{O}_{9+\delta}$ , and  $\text{Ca}_3\text{Co}_{4.4}\text{O}_{9+\delta}$  were prepared using a common solid-state reactions

method from calcium carbonate (“analytically pure grade”, min. 99.0 wt %, VEKTON, Russian Federation) and cobalt (II,III) oxide (“pure grade”, min. 99.0 wt%, VEKTON, Russian Federation) as precursors. The chemicals were taken in the molar ratios of 3:1.20, 3:1.33, and 3:1.47, respectively, homogenized by mixing in an agate mortar with addition of ethanol and then heated in air at 900 °C within 12 h in a muffle furnace according to the procedure described in detail in Refs. [26,29]. The sintered ceramic pellets with a diameter of 20 mm and a thickness of 2–3 mm were prepared by a FAST machine (DSP 507, Dr. Fritsch GmbH., Germany) in an argon atmosphere at 900 °C for 5 min under a pressure of 50 MPa. The heating and cooling rates were 100 °C·min<sup>-1</sup> and 50 °C·min<sup>-1</sup>, respectively. After the FAST sintering the sintered samples were additionally annealed in air at 700 °C for 14 h. Specimens in the form of bars with sizes of  $\approx 3 \times 3 \times 20 \text{ mm}^3$ ,  $\approx 3 \times 3 \times 4 \text{ mm}^3$ , and  $\approx 3 \times 3 \times 20 \text{ mm}^3$ , and in the form of pellets with a diameter of 13 mm and a thickness of 2–3 mm were cut from the sintered pellets for measuring their thermal expansion, electrical conductivity, the Seebeck coefficient, and thermal diffusivity.

The phase composition of the samples and crystal structure of their major phase ( $\text{Ca}_3\text{Co}_4\text{O}_{9+\delta}$ ) were studied by the XRD analysis (STOE Theta/Theta diffractometer (Germany),  $\text{CoK}_\alpha$ -radiation,  $\lambda = 1.78892 \text{ \AA}$ ). The patterns were collected at room temperature with a step size of 0.02° over the scanning angular range of 5–80° at 40 kV and 40 mA. The FTIR absorption spectra of the powders were measured within 300–1500 cm<sup>-1</sup> on a ThermoNicolet Nexus Fourier-Transform Infrared Spectrometer in KBr pellets.

The theoretical density of the samples ( $\rho_t$ ) was calculated as  $\rho_t = \sum \omega_i \cdot \rho_i$ , where  $\omega_i$  and  $\rho_i$  are mass fractions and X-ray densities of components of ceramics, which for  $\text{Ca}_3\text{Co}_4\text{O}_{9+\delta}$ ,  $\text{Ca}_3\text{Co}_2\text{O}_6$ , and  $\text{Co}_3\text{O}_4$  were equal to 4.68 g·cm<sup>-3</sup> [7], 4.498 g·cm<sup>-3</sup> (PDF–2, Card N° 00–051–0311), and 6.056 g·cm<sup>-3</sup> (PDF–2, Card N° 00–042–1467), respectively. The apparent density ( $\rho_{app}$ ) of ceramics was determined from their mass and geometrical sizes. The porosity of the samples ( $P$ ) was calculated as  $P = (1 - \rho_{app}/\rho_t) \cdot 100 \%$ .

The microstructure of the sintered ceramics and its chemical composition were studied by SEM with a JEOL JSM–7500F Field Emission Scanning Electron Microscope equipped with an EDS detector. The XPS spectra were recorded using an EA 15 hemispherical analyzer (PREVAC) equipped with an RS 40B1 dual anode X-ray source (PREVAC). MgK $\alpha$  (1254 eV) radiation was applied to generate core excitation. The electron binding energy (BE) scale was calibrated for the Fermi edge at 0.0 eV. The spectra were analyzed with the use of CasaXPS 2.3.15 software.

The thermal expansion, electrical conductivity ( $\sigma$ ), and the Seebeck coefficient ( $S$ ) of the sintered ceramics were measured in air within 25–825 °C according to the methods described in detail elsewhere [22,29,54]. Measurements were carried out in the direction perpendicular to the pressing axis ( $\Delta l/l_0$ ,  $\sigma_\perp$ ,  $S_\perp$ ), but electrical conductivity was studied also in the direction parallel to the pressing axis ( $\sigma_\parallel$ ,  $S_\parallel \approx S_\perp$ ).

Values of the average linear thermal expansion coefficient ( $\alpha$ , LTEC) and apparent activation energy of electrical conductivity ( $E_A$ ) were calculated from the linear parts of  $\Delta l/l_0 = f(T)$  and  $\ln(\sigma \cdot T) = f(1/T)$  plots, respectively. The power factor values of the studied samples were determined as  $PF = S^2 \cdot \sigma$  [4].

The thermal diffusivity ( $\eta$ ) of the samples was measured in the Ar atmosphere within the temperature interval of 15–835 °C by means of an LFA 457 MicroFlash (NETZSCH) device in the direction parallel to the pressure axis ( $\eta_\parallel$ ). The thermal conductivity values ( $\lambda$ ) of the ceramics were calculated according to the equation  $\lambda = \eta \cdot \rho_{app} \cdot C_p$ , where  $C_p$  is the heat capacity determined by the Dulong–Petit law. The phonon ( $\lambda_{ph}$ ) and electronic part ( $\lambda_{el}$ ) of thermal conductivity of ceramics were found by relations of  $\lambda = \lambda_{ph} + \lambda_{el}$ ,  $\lambda_{el} = L \cdot T \cdot \sigma$ , where  $L$  is the Lorentz number,  $L = 2.45 \cdot 10^{-8} \text{ V}^2 \cdot \text{K}^{-2}$ .

The figure-of-merit values of the samples were determined as  $ZT = PF \cdot T/\lambda$  [4].

### 3. Results and discussion

#### 3.1. Structural and microstructural characteristics of the synthesized layered cobaltites

The as-synthesized samples, except of  $\text{Ca}_3\text{Co}_4\text{O}_{9+\delta}$  compound, were non-single-phase materials as proved by the powder XRD patterns (Fig. 1). The  $\text{Ca}_{3.6}\text{Co}_4\text{O}_{9+\delta}$  and  $\text{Ca}_3\text{Co}_{4.4}\text{O}_{9+\delta}$  samples contained, along with the well-pronounced diffraction peaks of layered calcium cobaltite  $\text{Ca}_3\text{Co}_4\text{O}_{9+\delta}$  as the major phase [7], additional peaks assigned to the  $\text{Co}_3\text{O}_4$  phase (PDF–2, Card N<sup>o</sup> 00–042–1467) in  $\text{Ca}_3\text{Co}_{4.4}\text{O}_{9+\delta}$  sample, and the  $\text{Ca}_3\text{Co}_2\text{O}_6$  phase (PDF–2, Card N<sup>o</sup> 00–051–0311) in  $\text{Ca}_{3.6}\text{Co}_4\text{O}_{9+\delta}$  sample (Fig. 1).

The lattice constants of the major phase ( $\text{Ca}_3\text{Co}_4\text{O}_{9+\delta}$ ) in the ceramics with different compositions were close to each other (Table 1) and in the agreement with the literature data, according to which for  $\text{Ca}_3\text{Co}_4\text{O}_{9+\delta}$  the lattice constants are  $a = 4.8376(7)$  Å,  $b_1 = 4.5565(6)$  Å,  $b_2 = 2.8189(4)$  Å,  $c = 10.833(1)$  Å, and  $\beta = 98.061(1)^\circ$  (monoclinic syngony) [7]. Note that a slight increase in the constant  $a$  and  $V$  of the layered calcium cobaltite in the ceramics with a deviation of the Ca:Co ratio from stoichiometric one (3:4) was found. The constant  $b$  and the ratio of  $b_1/b_2$  slightly decreased when Ca:Co ratio was higher than 3:4 ( $\text{Ca}_3\text{Co}_{3.6}\text{O}_{9+\delta}$  compound), and the constant  $c$  and angle  $\beta$  slightly decreased when Ca:Co ratio was less than 3:4 ( $\text{Ca}_3\text{Co}_{4.4}\text{O}_{9+\delta}$  compound).

Fig. 2 presents the FTIR spectra of the powdered samples in the range  $300\text{--}800\text{ cm}^{-1}$ . Four absorption bands located at  $320\text{--}325\text{ cm}^{-1}$  ( $\nu_1$ ),  $572\text{--}582\text{ cm}^{-1}$  ( $\nu_2$ ),  $624\text{--}638\text{ cm}^{-1}$  ( $\nu_3$ ), and  $732\text{ cm}^{-1}$  ( $\nu_4$ ) corresponded to the bending ( $\nu_1$ ) and stretching ( $\nu_2\text{--}\nu_4$ ) vibrations of the Co–O bonds ( $\nu_1\text{--}\nu_3$ ) and Ca–O bonds ( $\nu_4$ ) in the structure of layered calcium cobaltite [17]. The FTIR absorption spectrum of the  $\text{Ca}_3\text{Co}_{4.4}\text{O}_{9+\delta}$  sample containing an excess of cobalt oxide ( $\text{Co}_3\text{O}_4$ ) (contained two additional absorption bands located at  $307\text{ cm}^{-1}$  ( $\nu_5$ ) and  $391\text{ cm}^{-1}$  ( $\nu_6$ ), which correspond to the stretching ( $\nu_5$ ) and bending ( $\nu_6$ ) vibrations of Co–O bonds in the cobalt oxide  $\text{Co}_3\text{O}_4$  [55]). The FTIR absorption spectrum of the sample deficient in cobalt oxide ( $\text{Ca}_3\text{Co}_{3.6}\text{O}_{9+\delta}$ ) had one additional band located at  $446\text{ cm}^{-1}$  ( $\nu_7$ ), corresponding to the stretching vibrations of Ca–O bonds in the  $\text{Ca}_3\text{Co}_2\text{O}_6$  phase [56].

The values of apparent density of the FAST sintered ceramics were equal to 4.22, 4.32, and  $4.13\text{ g cm}^{-3}$  for the samples with composition of  $\text{Ca}_{3.6}\text{Co}_4\text{O}_{9+\delta}$ ,  $\text{Ca}_3\text{Co}_4\text{O}_{9+\delta}$ , and  $\text{Ca}_3\text{Co}_{4.4}\text{O}_{9+\delta}$ , respectively, which corresponds to the porosity values of 9.2, 7.9, and 13.2% respectively. Obtained results show that: i) the FAST technique allows to prepare ceramics with low porosity ( $P < 10\%$ ), whereas  $\text{Ca}_3\text{Co}_4\text{O}_{9+\delta}$  ceramics, obtained by means of traditional ceramic method, possesses higher

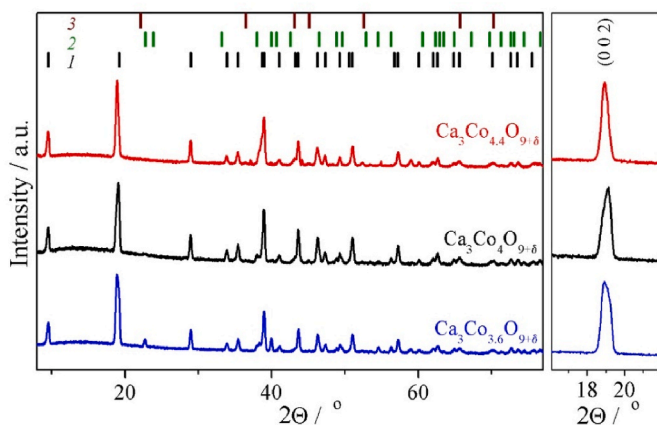


Fig. 1. XRD patterns of as-prepared samples at room temperature (Co–K $\alpha$  radiation). The panel to the right shows an enlarged view at  $2\theta$  16–22°. Reference Bragg positions correspond to (1)  $\text{Ca}_3\text{Co}_4\text{O}_{9+\delta}$  [7], (2)  $\text{Ca}_3\text{Co}_2\text{O}_6$  (PDF #00–051–0311), and (3)  $\text{Co}_3\text{O}_4$  (PDF #00–042–1467) phases.

Table 1

Lattice constants of the major phase (layered calcium cobaltite) in the ceramics.

Sample	$\text{Ca}_3\text{Co}_{3.6}\text{O}_{9+\delta}$	$\text{Ca}_3\text{Co}_4\text{O}_{9+\delta}$	$\text{Ca}_3\text{Co}_{4.4}\text{O}_{9+\delta}$
$a$ , Å	4.838	4.840	4.834
$b_1$ , Å	4.556	4.561	4.563
$b_2$ , Å	2.785	2.785	2.786
$c$ , Å	10.85	10.85	10.84
$\beta$ , °	98.46	98.46	98.29
$V$ , Å <sup>3</sup>	236.55	236.94	236.66
$b_1/b_2$	1.636	1.638	1.638

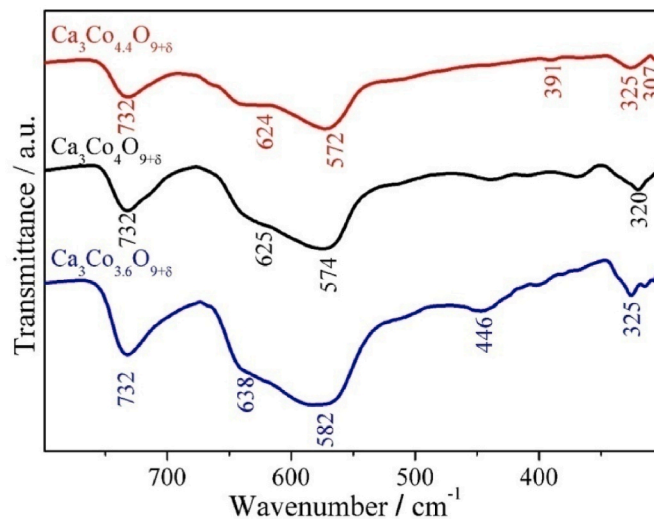


Fig. 2. FTIR spectra of the samples at room temperature.

porosity values, for example, 25% [33] or even 47% [29]); ii) the creation of the phase inhomogeneity in  $\text{Ca}_3\text{Co}_4\text{O}_{9+\delta}$ -based ceramics through its self-doping lowers not very significantly its sinterability.

The microstructure of  $\text{Ca}_3\text{Co}_{3.6}\text{O}_{9+\delta}$  and  $\text{Ca}_3\text{Co}_4\text{O}_{9+\delta}$  ceramics was layered and consisted of well-crystallized plates (flakes) of 8–10  $\mu\text{m}$  in size and thickness of about 1  $\mu\text{m}$ , which were partially aggregated in stacks and predominantly oriented in the direction perpendicular to the pressing axis. In the  $\text{Ca}_3\text{Co}_{4.4}\text{O}_{9+\delta}$  ceramics, the anisometric shape of the crystallites of the major phase of layered calcium cobaltite  $\text{Ca}_3\text{Co}_4\text{O}_{9+\delta}$  was less pronounced, the crystallite size varied in a wide range, and a part of crystallites was aggregated in stacks. In their neighborhood small (about 1  $\mu\text{m}$  in size) almost isometric particles of impurity phase  $\text{Co}_3\text{O}_4$  [45] could be seen (Fig. 3). The  $\text{Ca}_3\text{Co}_{4.4}\text{O}_{9+\delta}$  sample showed a large number of pores, in agreement with the results of the determination of the apparent density and porosity of the samples.

Additionally, the elemental composition of the surface in micro areas of the obtained materials was examined by the EDS method. Fig. 4 shows the surface regions selected for the analysis and their elemental compositions are summarized in Table 2. Examination of  $\text{Ca}_3\text{Co}_{3.6}\text{O}_{9+\delta}$  and  $\text{Ca}_3\text{Co}_4\text{O}_{9+\delta}$  samples showed some inconsistency with their nominal compositions. In both cases, this can be attributed to the phase inhomogeneity and the presence of the additional phases in  $\text{Ca}_3\text{Co}_{3.6}\text{O}_{9+\delta}$  ( $\text{Ca}_3\text{Co}_4\text{O}_9$  and  $\text{Ca}_3\text{Co}_2\text{O}_6$ ) and  $\text{Ca}_3\text{Co}_{4.4}\text{O}_9$  ( $\text{Ca}_3\text{Co}_4\text{O}_9$  and  $\text{Co}_3\text{O}_4$ ) materials. Moreover, a high relative Ca/Co ratio determined from the point analysis of the  $\text{Ca}_3\text{Co}_{3.6}\text{O}_{9+\delta}$  sample surface (Fig. 4, point 3) may indicate the presence of calcium carbonate on the surface. However, this impurity may originate from the unreacted precursor or the interaction of the surface with carbon dioxide from the air. In turn, the relative Ca/Co ratio in  $\text{Ca}_3\text{Co}_4\text{O}_{9+\delta}$  sample was similar in all examined points. It is worth noting, however, that all elements were evenly distributed on the obtained surfaces as indicated by the results of EDS mapping of the ceramic surface (Figs. S1–S3 in the online supplementary material).

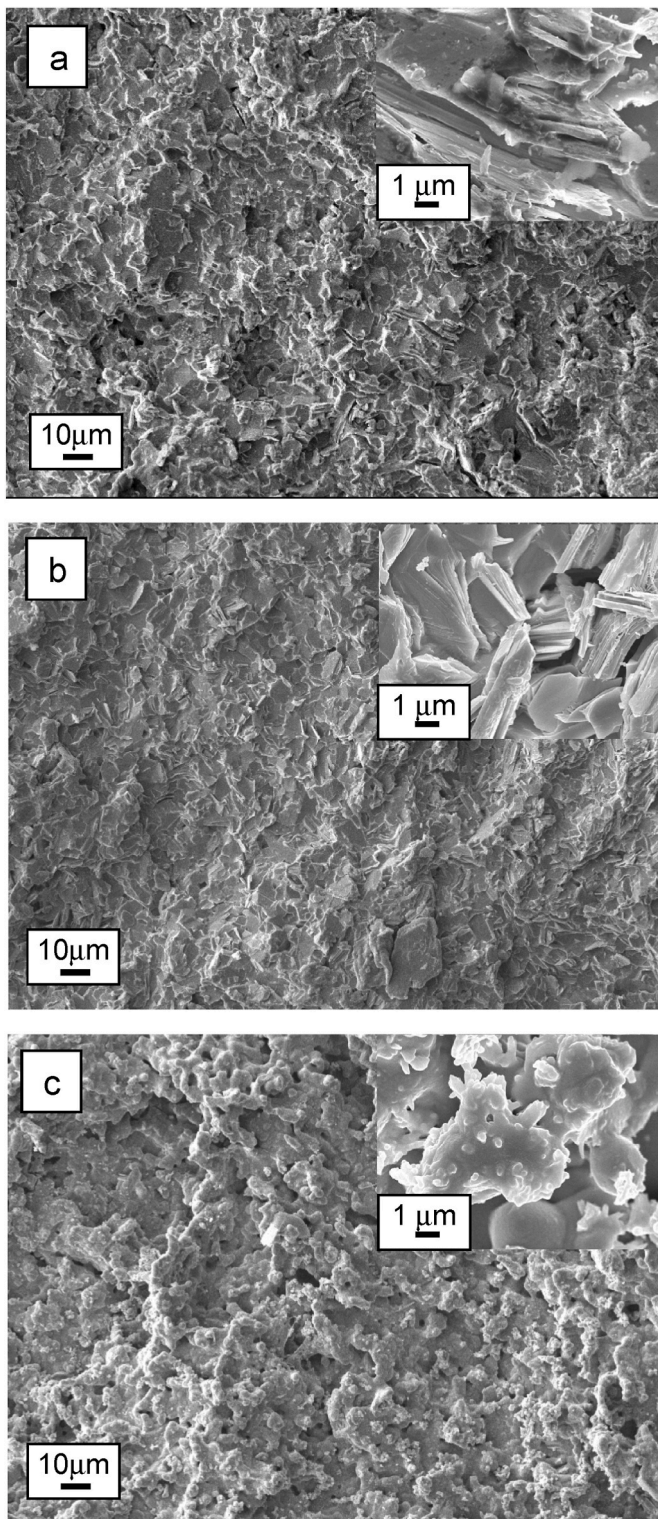


Fig. 3. SEM images of the fractured surface of  $\text{Ca}_3\text{Co}_{3.6}\text{O}_{9+\delta}$  (a),  $\text{Ca}_3\text{Co}_4\text{O}_{9+\delta}$  (b), and  $\text{Ca}_3\text{Co}_{4.4}\text{O}_{9+\delta}$  (c) samples prepared by FAST.

In order to identify the valence states of constituents in the obtained materials, high-resolution XPS spectra were registered (Fig. 5). The shapes of the spectra of all materials were similar and mostly differed only by the relative contribution of the components. The Ca2p high-resolution XPS spectra were deconvoluted into 3 peak doublets (Fig. 5a), each corresponding to Ca2p<sub>3/2</sub> and Ca2p<sub>1/2</sub> signals. The first component, Ca<sub>(1)</sub>, which has the main Ca2p<sub>3/2</sub> peak located at ca. 345

eV and the second component, Ca<sub>(2)</sub>, located at ca. 346 eV were assigned to Ca–O compounds in two different chemical environments in the lattice structure of the obtained ceramics [57,58]. The third component, Ca<sub>(3)</sub>, was assigned to surface carbonates, which is in good agreement with the SEM/EDS data (Fig. 4 and Table 2).

The Co2p high-resolution XPS spectra (Fig. 5b) were also deconvoluted into 3 peak doublets in Co2p<sub>3/2</sub> and Co2p<sub>1/2</sub> regions. The components Co<sub>(1)</sub> (ca. 779 eV), Co<sub>(2)</sub> (ca. 780 eV), and Co<sub>(3)</sub> (ca. 782 eV) were assigned to the valence states Co<sup>2+</sup>, Co<sup>3+</sup>, and Co<sup>4+</sup>, respectively [6,59,60]. The shake-up satellite peaks of  $\pi^*$  electrons, marked as sat. in Fig. 5b were also observed, confirming the presence of Co<sup>2+</sup> (ca. 785 eV) and Co<sup>3+</sup> (ca. 789 eV) in synthesized compounds [61].

In the case of the O1s high-resolution spectra (Fig. 5c), two main components O<sub>(1)</sub> (ca. 529 eV), O<sub>(2)</sub> (ca. 531 eV), and a minor component O<sub>(3)</sub> (ca. 532.5 eV) were deconvoluted. The components O<sub>(1)</sub> and O<sub>(2)</sub> were associated with the Co–O and Ca–O compounds, respectively [58, 59]. The O<sub>(3)</sub> component was due to adsorbed water and possible organic contaminants from the atmosphere [58]. The relative content of each component in the examined materials was evaluated based on the peak areas and the results are summarized in Table 3. The relative ratio of O<sub>(1)</sub>/O<sub>(2)</sub> peaks, which can be attributed to the Co–O/Ca–O ratio increased for  $\text{Ca}_3\text{Co}_4\text{O}_{9+\delta}$  and  $\text{Ca}_3\text{Co}_{4.4}\text{O}_{9+\delta}$  compared to  $\text{Ca}_3\text{Co}_{3.6}\text{O}_{9+\delta}$ . However, a small decrease in the relative ratio of O<sub>(1)</sub>/O<sub>(2)</sub> peaks between  $\text{Ca}_3\text{Co}_4\text{O}_{9+\delta}$  and  $\text{Ca}_3\text{Co}_{4.4}\text{O}_{9+\delta}$  can be assigned to the presence of the second phases in the latter sample.

### 3.2. Electrical, thermal, and thermoelectric characteristics of the synthesized layered cobaltites

The electrical conductivity of the cobaltite ceramics at temperatures close to the room temperature had metallic character ( $\partial\sigma/\partial T < 0$ ), which changed into semiconducting one ( $\partial\sigma/\partial T > 0$ ) near 225 °C (Fig. 6). This behavior was attributed to the metal–semiconductor phase transition of  $\text{Ca}_3\text{Co}_4\text{O}_{9+\delta}$ , which occurs at this temperature [62]. Note that values of electrical conductivity of ceramics measured in the direction perpendicular to the pressing axis ( $\sigma_{\perp}$ ) were 1.4–4.1 times larger than those found in the direction parallel to the pressing axis ( $\sigma_{\parallel}$ ) (Fig. 6, Table 4). It is known that the electrical conductivity of  $\text{Ca}_3\text{Co}_4\text{O}_{9+\delta}$  single crystals is strongly anisotropic ( $\sigma_{ab}/\sigma_c = 500\text{--}1000$ ) [8] and for textured ceramics based on the layered calcium cobaltite, ratio  $\sigma_{\perp}/\sigma_{\parallel} \approx 13.5$  at 25 °C, 8.8 at 625 °C K [13], and 6–8 at 525 °C [14]. Therefore, the results of electrical conductivity measurements prove the texturing of ceramics prepared by the FAST and applying pressure of 50 MPa during sintering, obtained in this work. The values of the electrical conductivity of the samples prepared by the FAST technique (except  $\sigma_{\parallel}$  values of  $\text{Ca}_3\text{Co}_{3.6}\text{O}_{9+\delta}$ ) were essentially higher ( $\sigma \approx 40\text{--}140 \text{ S cm}^{-1}$ ) than those for ceramics prepared using solid–state reactions or citrate methods followed by conventional sintering ( $\sigma \approx 20\text{--}25 \text{ S cm}^{-1}$  [26,29,33,45]) due to their low porosity. Moreover, the conductivity of the samples strongly increased with increasing the cobalt oxide ( $\text{Co}_3\text{O}_4$ ) content. For the non-single phase  $\text{Ca}_3\text{Co}_{4.4}\text{O}_{9+\delta}$  ceramics containing  $\text{Co}_3\text{O}_4$  as impurity phase,  $\sigma_{\perp}$  values throughout the studied temperature interval were 40–60 % larger than those for the single-phase  $\text{Ca}_3\text{Co}_4\text{O}_{9+\delta}$  sample (Fig. 6).

The values of apparent activation energy of electrical conductivity of ceramics in the temperature range of 325–825 °C varied within 81–124 meV (Table 4), which coincides well with the values of  $E_A = 83\text{--}91 \text{ meV}$  for  $(\text{Ca},\text{La})_3\text{Co}_4\text{O}_{9+\delta}$  single-phase ceramics [62] and  $E_A$  of 86–136 meV for  $\text{Ca}_{2.4}\text{Co}_4\text{O}_{9+\delta}\text{--}\text{Ca}_3\text{Co}_{3.4}\text{O}_{9+\delta}$  composites [22]. This fact indicates the common mechanism of electrical conductivity in these materials, which is determined by the charge transfer within the  $\text{Ca}_3\text{Co}_4\text{O}_{9+\delta}$  major phase of the samples.

The sign of the Seebeck coefficient of studied materials was positive ( $S > 0$ ), indicating that holes are the main charge carriers and these compounds are p-type conductors. The values of the Seebeck coefficient of ceramics increased almost linearly as the temperature increased and

**Table 2**  
EDX point elemental analysis of obtained ceramics.

Elemental composition, at.%									
Sample	Ca <sub>3</sub> Co <sub>3.6</sub> O <sub>9+δ</sub>			Ca <sub>3</sub> Co <sub>4</sub> O <sub>9+δ</sub>			Ca <sub>3</sub> Co <sub>4.4</sub> O <sub>9+δ</sub>		
	1	2	3	4	5	6	7	8	9
Point in Fig. 4									
Ca	15.6	19.8	15.9	22.5	22.9	22.9	17.9	16.8	24.0
Co	20.3	12.8	3.5	14.4	14.2	14.1	24.2	23.2	35.2
O	64.1	67.4	80.6	63.1	62.9	63.0	57.9	60.0	40.8

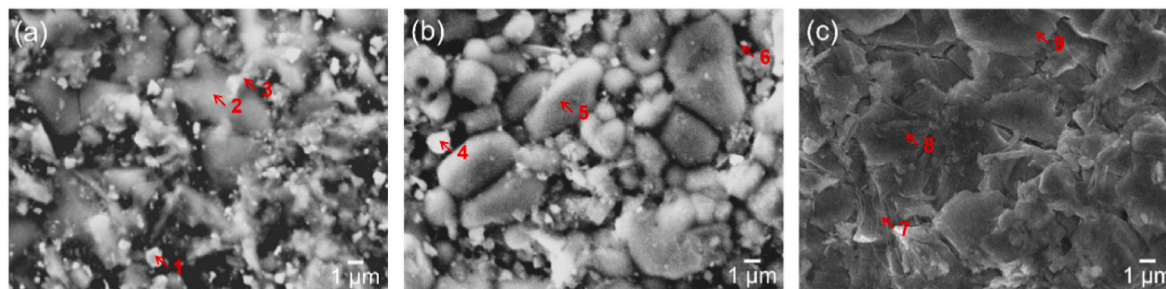


**Fig. 4.** SEM images of Ca<sub>3</sub>Co<sub>3.6</sub>O<sub>9+δ</sub> (a), Ca<sub>3</sub>Co<sub>4</sub>O<sub>9+δ</sub> (b), and Ca<sub>3</sub>Co<sub>4.4</sub>O<sub>9+δ</sub> (c) samples showing regions of the EDX analysis listed in Table 2.

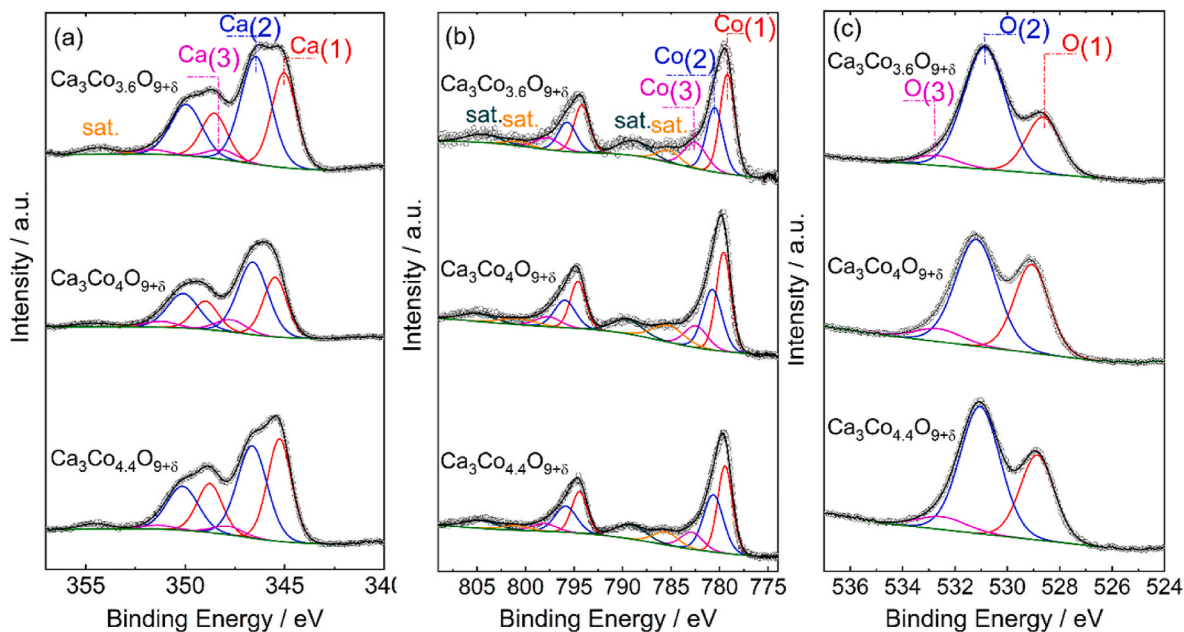


**Fig. 5.** High-resolution XPS spectra of obtained materials registered in the binding energy range of Ca2p (a), Co2p (b), and O1s (c).

**Table 3**  
Relative surface composition of the examined ceramics based on XPS analysis of element binding energies (BE).

	Ca2p <sub>3/2</sub>			Co2p <sub>3/2</sub>			O1s		
	Ca(1)	Ca(2)	Ca(3)	Co(1)	Co(2)	Co(3)	O(1)	O(2)	O(3)
Ca <sub>3</sub> Co <sub>3.6</sub> O <sub>9+δ</sub>									
BE, eV	345.04	346.45	348.16	779.20	780.51	782.52	528.64	530.87	532.69
Composition, %	40.0	55.1	4.9	47.3	34.1	18.6	25.9	68.5	5.6
Ca <sub>3</sub> Co <sub>4</sub> O <sub>9+δ</sub>									
BE, eV	345.48	346.60	347.72	779.60	780.75	782.44	529.07	531.19	532.62
Composition, %	35.7	55.0	9.3	47.0	37.1	15.9	37.6	54.9	7.5
Ca <sub>3</sub> Co <sub>4.4</sub> O <sub>9+δ</sub>									
BE, eV	345.26	346.64	347.84	779.44	780.65	782.86	528.86	531.04	532.51
Composition, %	44.9	50.5	4.6	46.1	40.7	13.2	33.6	59.1	7.3

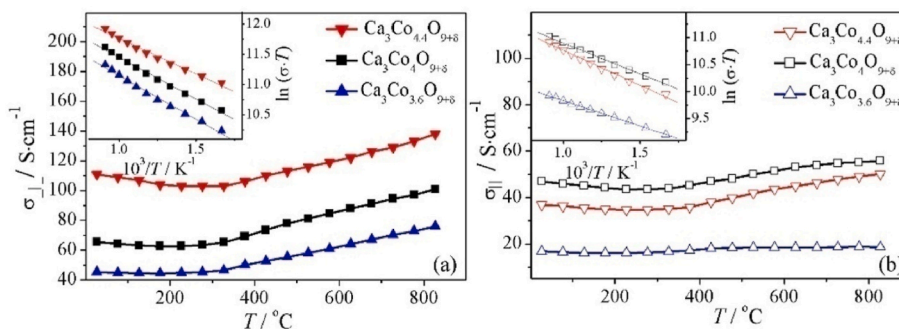


Fig. 6. Temperature dependences of electrical conductivity of the samples measured perpendicular ( $\sigma_{\perp}$ ) (a) and parallel ( $\sigma_{\parallel}$ ) (b) to the pressing axis. Insets show the corresponding Arrhenius plots of electrical conductivity.

Table 4  
Electrical conductivity parameters of ceramics.

Sample	$(\sigma_{\perp}/\sigma_{\parallel})_{300}$	$(\sigma_{\perp}/\sigma_{\parallel})_{1100}$	$E_{A,\parallel}$ , meV	$E_{A,\perp}$ , meV	$E_{A,\perp}/E_{A,\parallel}$
$\text{Ca}_3\text{Co}_{3.6}\text{O}_{9+\delta}$	2.70	4.09	81(1)	124(4)	1.53
$\text{Ca}_3\text{Co}_4\text{O}_{9+\delta}$	1.40	1.81	98(2)	118(3)	1.20
$\text{Ca}_3\text{Co}_{4.4}\text{O}_{9+\delta}$	3.01	2.75	112(3)	101(4)	0.90

for the samples with cationic nonstoichiometry ( $\text{Ca}_3\text{Co}_{3.6}\text{O}_{9+\delta}$  and  $\text{Ca}_3\text{Co}_{4.4}\text{O}_{9+\delta}$ ) containing an excess amount of calcium or cobalt oxides were essentially larger (by 5–20% depending on temperature and composition) than for cation stoichiometric single-phase  $\text{Ca}_3\text{Co}_4\text{O}_{9+\delta}$  sample (Fig. 7a). The maximum value of  $S$  192  $\mu\text{V}\cdot\text{K}^{-1}$  at 825°C possessed  $\text{Ca}_3\text{Co}_{3.6}\text{O}_{9+\delta}$  sample, which consisted of  $\text{Ca}_3\text{Co}_4\text{O}_{9+\delta}$  and  $\text{Ca}_3\text{Co}_2\text{O}_6$ .

Similar results were found earlier in Refs. [22,49], where it was shown that the values of the Seebeck coefficient of non-single-phase ceramics in  $\text{Ca}_{2.4}\text{Co}_4\text{O}_{9+\delta}$ – $\text{Ca}_3\text{Co}_{3.4}\text{O}_{9+\delta}$  [22],  $\text{Ca}_3\text{Co}_4\text{O}_9/\text{Ca}_3\text{Co}_2\text{O}_6$  [49] systems were appreciably higher than for single-phase  $\text{Ca}_3\text{Co}_4\text{O}_{9+\delta}$  material. In our earlier work [29,45], we have also observed a significant growth of the Seebeck coefficient values of  $\text{Ca}_{3-x}\text{Bi}_x\text{Co}_4\text{O}_{9+\delta}$  ceramics at the transition from single-phase  $\text{Ca}_{3-x}\text{Bi}_x\text{Co}_4\text{O}_{9+\delta}$  solid solutions to the phase-heterogeneous samples containing  $\text{Ca}_{2.7}\text{Bi}_{0.3}\text{Co}_4\text{O}_{9+\delta}$ ,  $\text{Bi}_2\text{Ca}_2\text{Co}_{1.7}\text{O}_y$ , and  $\text{Co}_3\text{O}_4$  phases. Therefore, it can be concluded that the creation of phase heterogeneity in the ceramics based on the  $\text{Ca}_3\text{Co}_4\text{O}_{9+\delta}$  appreciably increases their Seebeck coefficient, particularly owing to the introduction of less conducting  $\text{Ca}_3\text{Co}_2\text{O}_6$  or  $\text{Co}_3\text{O}_4$  phases.

The power factor values of sintered ceramics increased with temperature, and the most pronouncing growth of  $PF$  was observed at high temperatures at which samples possessed the semiconducting character of electrical conductivity (Fig. 7b). The values of  $PF$  of samples in the direction parallel to the pressing axis were less than in the direction perpendicular to the pressing axis due to  $\sigma_{\perp} > \sigma_{\parallel}$  (Fig. 6, Table 4). For

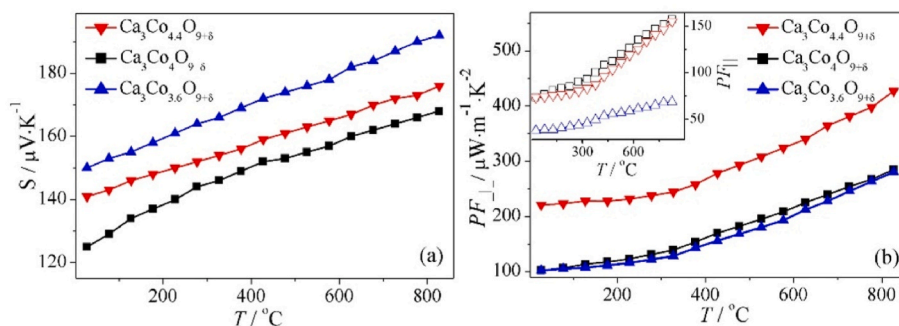


Fig. 7. Temperature dependences of the Seebeck coefficient (a) and power factor (b) values of  $\text{Ca}_3\text{Co}_{3.6}\text{O}_{9+\delta}$ ,  $\text{Ca}_3\text{Co}_4\text{O}_{9+\delta}$ , and  $\text{Ca}_3\text{Co}_{4.4}\text{O}_{9+\delta}$  ceramics, prepared by FAST technique, in direction perpendicular and parallel (inset) to the pressing axis.

$\text{Ca}_3\text{Co}_{3.6}\text{O}_{9+\delta}$  and  $\text{Ca}_3\text{Co}_4\text{O}_{9+\delta}$  samples,  $PF_{\perp}$  values were close to each other and for  $\text{Ca}_3\text{Co}_{4.4}\text{O}_{9+\delta}$  they were essentially larger, which is due to the high values both of its electrical conductivity and the Seebeck coefficient. The highest power factor of 427  $\mu\text{W}\cdot\text{m}^{-1}\cdot\text{K}^{-2}$  at 825°C in the direction perpendicular to the pressing axis showed non-single phase  $\text{Ca}_3\text{Co}_{4.4}\text{O}_{9+\delta}$  ceramics, containing  $\text{Ca}_3\text{Co}_4\text{O}_{9+\delta}$  and  $\text{Co}_3\text{O}_4$ . This value is 1.5 times higher than for the single-phase  $\text{Ca}_3\text{Co}_4\text{O}_{9+\delta}$  sample prepared using the same method ( $PF_{\perp,825} = 280 \mu\text{W}\cdot\text{m}^{-1}\cdot\text{K}^{-2}$ ) and more than 4 times higher than for highly porous  $\text{Ca}_3\text{Co}_4\text{O}_{9+\delta}$  ceramics synthesized by the traditional ceramics preparation method followed by conventional sintering ( $PF_{825} \approx 100 \mu\text{W}\cdot\text{m}^{-1}\cdot\text{K}^{-2}$ ) [26,29,33,45].

Dependences  $\Delta l/l_0 = f(T)$  for the studied ceramics were linear, suggesting the absence of the structural phase transition of its main  $\text{Ca}_3\text{Co}_4\text{O}_{9+\delta}$  phase in the temperature range of 25–825°C, which coincides with the literature data [26,29,33,52]. The values of LTEC were equal to  $12.3(2)\cdot 10^{-6} \text{K}^{-1}$ ,  $12.2(1)\cdot 10^{-6} \text{K}^{-1}$ , and  $12.4(2)\cdot 10^{-6} \text{K}^{-1}$  for  $\text{Ca}_3\text{Co}_{3.6}\text{O}_{9+\delta}$ ,  $\text{Ca}_3\text{Co}_4\text{O}_{9+\delta}$ , and  $\text{Ca}_3\text{Co}_{4.4}\text{O}_{9+\delta}$  samples, respectively. The LTEC values of sintered ceramics using the FAST method were noticeably smaller than those for  $\text{Ca}_3\text{Co}_4\text{O}_{9+\delta}$  obtained using conventional sintering ( $12.8\cdot 10^{-6} \text{K}^{-1}$ ) [26,29,33] due to their smaller porosity. For cation nonstoichiometric samples ( $\text{Ca}_3\text{Co}_{3.6}\text{O}_{9+\delta}$ ,  $\text{Ca}_3\text{Co}_{4.4}\text{O}_{9+\delta}$ ) LTECs were slightly larger than for cation stoichiometric one ( $\text{Ca}_3\text{Co}_4\text{O}_{9+\delta}$ ), probably due to their phase inhomogeneity.

The values of thermal diffusivity and thermal conductivity of the rapidly hot-pressed ceramic samples determined in the direction parallel to the pressure axis decreased with the increasing temperature and were minimal for the  $\text{Ca}_3\text{Co}_{4.4}\text{O}_{9+\delta}$  sample (Fig. 8a), having the highest porosity among the materials studied and containing small particles of  $\text{Co}_3\text{O}_4$  secondary phase (Fig. 3), which resulted in the increase of density of grain boundaries, serving as effective areas of phonon scattering. The  $\lambda$  values of this material within the studied temperature interval were 18–22% and 25–29% less than for  $\text{Ca}_3\text{Co}_4\text{O}_{9+\delta}$  calcium cobaltite and  $\text{Ca}_3\text{Co}_{3.6}\text{O}_{9+\delta}$  composite, respectively.

The electronic part of the thermal conductivity of the studied

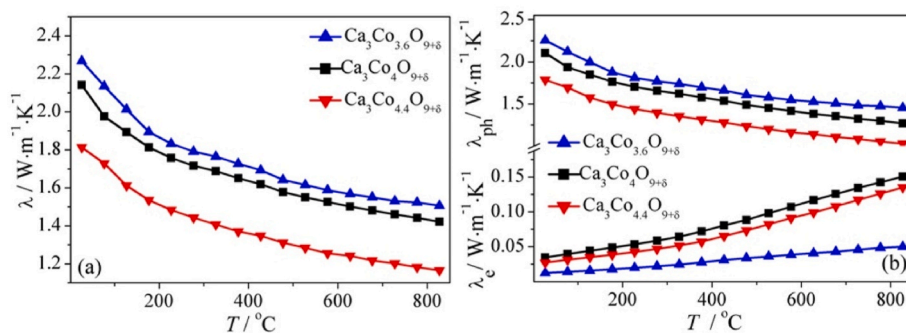


**Fig. 8.** Temperature dependences of the thermal conductivity (a) and phonon and electronic parts of thermal conductivity (b) values of  $\text{Ca}_3\text{Co}_{3.6}\text{O}_{9+\delta}$ ,  $\text{Ca}_3\text{Co}_4\text{O}_{9+\delta}$  and  $\text{Ca}_3\text{Co}_{4.4}\text{O}_{9+\delta}$  ceramics.

compounds increased with increasing temperature and was about 0.5–1.6% and 3.3–11.6% of the total thermal conductivity of the samples at 25°C and 825°C, respectively (Fig. 8b). The phonon part of the thermal conductivity dominated and decreased with increasing temperature (Fig. 8b).

To provide insight into the thermal transport behavior of the ceramics, the  $\lambda_{\text{ph}} = f(1/T)$  dependencies were plotted (Fig. 9) [63,64]. As can be seen, above 300°C the function  $\lambda_{\text{ph}} = f(1/T)$  is linear for all the samples, which points out the “Umklapping” process, indicating that the phonon–phonon interactions dominate [64]. Below 300°C the thermal conductivity is controlled by interface scattering, including grain boundary scattering [63]. Note that the transition temperature (300°C) is in a good agreement with the value of Debye temperature (299°C) calculated for the layered calcium cobaltite using the Debye model [65].

The figure-of-merit ( $ZT$ ) values of the samples calculated for the direction parallel to the pressure direction sharply increased with the increasing temperature (Fig. 10) and for  $\text{Ca}_3\text{Co}_{4.4}\text{O}_{9+\delta}$  material possessing the maximal thermoelectric performance reached  $ZT = 0.146$  at 825°C, which is by 20 and 192% higher than those for single-phase  $\text{Ca}_3\text{Co}_4\text{O}_{9+\delta}$  layered calcium cobaltite and  $\text{Ca}_3\text{Co}_{3.6}\text{O}_{9+\delta}$  composite materials, respectively.

Table 5 summarizes main parameters of ceramics obtained in this work and compares them with the literature data on  $\text{Ca}_3\text{Co}_4\text{O}_{9+\delta}$ -based ceramics of different compositions obtained by various techniques. The proposed combined approach of self-doping and innovative FAST technique allowed to obtain thermoelectric ceramics possessing improved functional properties without essential complication of their chemical and phase composition.

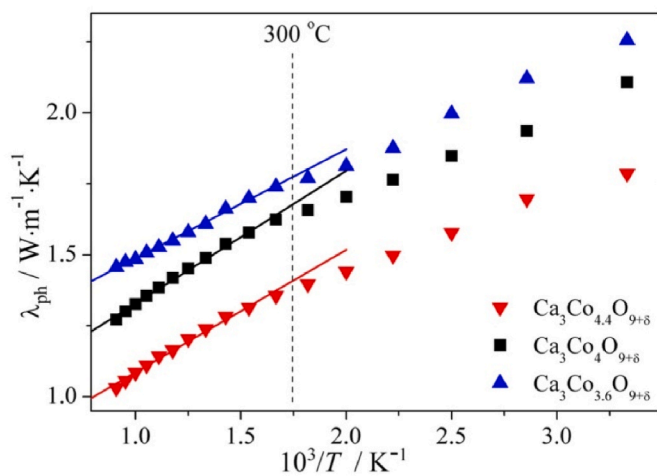


**Fig. 9.** Dependences of the phonon part of the thermal conductivity of  $\text{Ca}_3\text{Co}_{3.6}\text{O}_{9+\delta}$ ,  $\text{Ca}_3\text{Co}_4\text{O}_{9+\delta}$ , and  $\text{Ca}_3\text{Co}_{4.4}\text{O}_{9+\delta}$  samples versus reciprocal temperature.

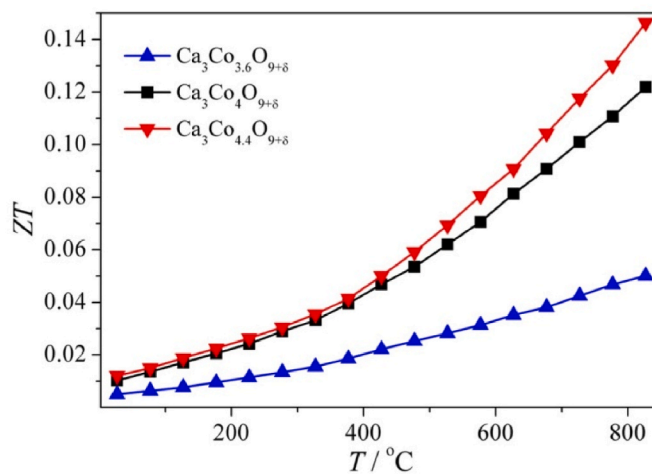


**Fig. 10.** Temperature dependences of the figure-of-merit values of  $\text{Ca}_3\text{Co}_{3.6}\text{O}_{9+\delta}$ ,  $\text{Ca}_3\text{Co}_4\text{O}_{9+\delta}$ , and  $\text{Ca}_3\text{Co}_{4.4}\text{O}_{9+\delta}$  ceramic samples prepared by FAST technique.

#### 4. Conclusions

The formation of phase inhomogeneity in ceramics based on the layered calcium cobaltite through its self-doping allowed to essentially increase in the Seebeck coefficient. The value of  $S$  for the sample self-doped with calcium oxide ( $\text{Ca}_3\text{Co}_{3.6}\text{O}_{9+\delta}$ ), containing  $\text{Ca}_3\text{Co}_2\text{O}_6$  as the secondary phase, in comparison to the single-phase  $\text{Ca}_3\text{Co}_4\text{O}_{9+\delta}$  ceramics increases more than for the samples self-doped with  $\text{Co}_3\text{O}_4$  oxide, containing  $\text{Co}_3\text{O}_4$  as secondary phase, and reaches  $192 \mu\text{V}\cdot\text{K}^{-1}$  at 825°C. Electric field assisted sintering technique with applied pressure of 50 MPa during sintering allows to obtain low porous ( $P = 8\text{--}13\%$ ) partially textured ceramics with larger values of electrical conductivity than for quasi-isotropic highly porous ceramics obtained using the traditional pressureless sintering method. The  $\text{Ca}_3\text{Co}_{4.4}\text{O}_{9+\delta}$  ceramics demonstrated the maximum electrical conductivity values of  $138 \text{ S}\cdot\text{cm}^{-1}$  at 825°C in the direction perpendicular to the pressing axis. The thermal conductivity of the samples below 300°C is controlled by interface scattering, but above 300°C the phonon–phonon interactions dominate. The minimal value of the thermal conductivity possessed the  $\text{Ca}_3\text{Co}_{4.4}\text{O}_{9+\delta}$  heterogeneous ceramics ( $1.166 \text{ W}\cdot\text{m}^{-1}\cdot\text{K}^{-1}$  at 825°C) in the direction parallel to the pressure axis which is 22% less than for  $\text{Ca}_3\text{Co}_4\text{O}_{9+\delta}$  layered calcium cobaltite. Joint use of self-doping and the FAST technique leads to the formation of thermoelectric oxide ceramics with improved functional characteristics. Among the samples studied in this work, the phase heterogeneous  $\text{Ca}_3\text{Co}_{4.4}\text{O}_{9+\delta}$  ceramics containing  $\text{Co}_3\text{O}_4$  as the secondary phase, possesses the highest power factor value of  $427 \mu\text{W}\cdot\text{m}^{-1}\cdot\text{K}^{-2}$  at 825°C in the direction perpendicular to the pressing axis,

Table 5

Comparison of literature-reported functional characteristics of Ca<sub>3</sub>Co<sub>4</sub>O<sub>9+δ</sub>-based ceramics obtained using various techniques with the results reported in this study.

Material	Sintering	$T_{\text{sint}}$ , °C	$P_{\text{sint}}$ , MPa	$P$ , %	$T$ , °C	$\sigma_T$ , S·cm <sup>-1</sup>	$S_T$ , μV·K <sup>-1</sup>	$PF_T$ , μW·m <sup>-1</sup> ·K <sup>-2</sup>	$\lambda_T$ , W·m <sup>-1</sup> ·K <sup>-1</sup>	$ZT_T$	Ref.
Ca <sub>3</sub> Co <sub>4</sub> O <sub>9+δ</sub>	SPS	850	50	–	800	67	150	100	2.6	0.10	[10]
Ca <sub>3</sub> Co <sub>4</sub> O <sub>9+δ</sub>	SPS	750	50	1	700	110	173	351	2.1	0.16	[16]
Ca <sub>3</sub> Co <sub>4</sub> O <sub>9+δ</sub>	OPS	800	25 ± 3	9	750	100	189	356	2.05	0.18	[19]
Ca <sub>3</sub> Co <sub>4</sub> O <sub>9+δ</sub>	TSS	1200	–	–	600	80	165	170	2.5	0.06	[20]
Ca <sub>3</sub> Co <sub>4</sub> O <sub>9+δ</sub>	CS	920	–	–	–	65	160	150	1.1	0.11	
(Ca <sub>0.87</sub> Ag <sub>0.1</sub> La <sub>0.03</sub> ) <sub>3</sub> Co <sub>4</sub> O <sub>9+δ</sub> /6 wt% B <sub>2</sub> O <sub>3</sub>	TSS	1100	–	2	800	85	181	280	0.94	0.30	[21]
Ca <sub>3</sub> Co <sub>4</sub> O <sub>9+δ</sub> /3 wt% Cu	TSS	1000	–	20	827	82	202	335	–	–	[23]
Ca <sub>3</sub> Co <sub>4</sub> O <sub>9+δ</sub>	CS	910	–	43	773	32	172	93	–	–	[29]
Ca <sub>3</sub> Co <sub>4</sub> O <sub>9+δ</sub> /0,25 wt% TiC	CS	900	–	26	800	60	194	224	2.1	0.16	[50]
Ca <sub>3</sub> Co <sub>4</sub> O <sub>9+δ</sub>	FAST	900	50	13	825	138	176	427	1.17	0.146	This
Ca <sub>3</sub> Co <sub>4</sub> O <sub>9+δ</sub>				8	825	101	168	280	1.42	0.122	work

which is 1.5 times higher than for single-phase FAST-sintered Ca<sub>3</sub>Co<sub>4</sub>O<sub>9+δ</sub> ( $PF_{\perp,825} = 280 \mu\text{W}\cdot\text{m}^{-1}\cdot\text{K}^{-2}$ ) and more than 4 times higher than for low density ( $P = 25\%$ ) Ca<sub>3</sub>Co<sub>4</sub>O<sub>9+δ</sub> ceramics prepared by conventional sintering ( $PF_{825} \approx 100 \mu\text{W}\cdot\text{m}^{-1}\cdot\text{K}^{-2}$  [23,26,29,45]). Figure-of-merit of Ca<sub>3</sub>Co<sub>4</sub>O<sub>9+δ</sub> ceramics in the direction parallel to the pressure axis at 825°C reaches 0.146, which is 20% more than of Ca<sub>3</sub>Co<sub>4</sub>O<sub>9+δ</sub> layered calcium cobaltite and 192% higher than of Ca<sub>3</sub>Co<sub>3.6</sub>O<sub>9+δ</sub> composite at the same temperature. Obtained results show high efficiency of using combined self-doping and FAST approach in obtaining the Ca<sub>3</sub>Co<sub>4</sub>O<sub>9+δ</sub>-based ceramics with enhanced thermoelectric performance without essential complication of its phase and chemical composition.

#### Data availability

The raw/processed data required to reproduce the findings of this study are available from the corresponding authors upon request.

#### CRediT authorship contribution statement

**Andrei I. Klyndyuk:** Writing – original draft, Validation, Supervision, Resources, Project administration, Methodology, Funding acquisition, Data curation, Conceptualization. **Dzmitry S. Kharytonau:** Writing – review & editing, Writing – original draft, Visualization, Validation, Resources, Investigation, Formal analysis, Data curation. **Iryna V. Matsukevich:** Writing – original draft, Validation, Investigation, Funding acquisition, Formal analysis. **Ekaterina A. Chizhova:** Visualization, Validation, Investigation, Formal analysis, Data curation. **Zoltán Lenčes:** Writing – review & editing, Resources, Investigation, Funding acquisition, Formal analysis. **Robert P. Socha:** Resources, Investigation, Formal analysis. **Małgorzata Zimowska:** Writing – review & editing, Investigation, Formal analysis. **Ondrej Hanzel:** Resources, Investigation, Funding acquisition, Formal analysis. **Marián Janek:** Writing – review & editing, Supervision, Resources, Project administration, Funding acquisition.

#### Declaration of competing interest

The authors declare that they have no known competing financial interests or personal relationships that could have appeared to influence the work reported in this paper.

#### Acknowledgements

Andrei I. Klyndyuk and Ekaterina A. Chizhova acknowledge financial support by the Ministry of Education of the Republic of Belarus (State Research Program “Physical Materials Science, New Materials and Technologies”, subprogram “Materials Science and Materials Technologies”, task “Development and Study of Composite Thermoelectrics Based on Layered Calcium Cobaltite”). Iryna V. Matsukevich

acknowledges financial support by the National Scholarship Program of the Slovak Republic and European Union Horizon 2020 Research and Innovation Program under grant agreement No. 739566. Marián Janek acknowledges the financial support by the Slovak Scientific Grant Agency (grants VEGA No. 1/0070/22, 1/0342/21). Zoltán Lenčes and Ondrej Hanzel acknowledge the financial support by the Slovak Scientific Grant Agency (grant VEGA No. 2/0007/21).

#### Appendix A. Supplementary data

Supplementary data to this article can be found online at <https://doi.org/10.1016/j.ceramint.2024.05.402>.

#### References

- [1] K. Biswas, J. He, I.D. Blum, C.-I. Wu, T.P. Hogan, D.N. Seidman, V.P. Dravid, M. G. Kanatzidis, High-performance bulk thermoelectrics with all-scale hierarchical architectures, *Nature* 489 (2012) 414–418, <https://doi.org/10.1038/nature11439>.
- [2] X. Wang, X. Liu, W. Yan, S. Hou, X. Li, Significant enhancement in Seebeck coefficient and power factor of Ca<sub>3</sub>Co<sub>4</sub>O<sub>9</sub> thermoelectric ceramics by SiC addition, *J. Alloys Compd.* 785 (2019) 698–705, <https://doi.org/10.1016/j.jallcom.2019.01.239>.
- [3] Y. Zhou, L.-D. Zhao, Promising thermoelectric bulk materials with 2D structures, *Adv. Mater.* 29 (2017) 1702676, <https://doi.org/10.1002/adma.201702676>.
- [4] K. Koumoto, R. Funahashi, E. Guilmeau, Y. Miyazaki, A. Weidenkaff, Y. Wang, C. Wan, Thermoelectric ceramics for energy harvesting, *J. Am. Ceram. Soc.* 96 (2013) 1–23, <https://doi.org/10.1111/jace.12076>.
- [5] J.W. Fergus, Oxide materials for high temperature thermoelectric energy conversion, *J. Eur. Ceram. Soc.* 32 (2012) 525–540, [10.1016/j.jeurceramsoc.2011.10.007](https://doi.org/10.1016/j.jeurceramsoc.2011.10.007).
- [6] Y. Huang, B. Zhao, S. Lin, Y. Sun, Enhanced thermoelectric performance induced by misplaced substitution in layered Ca<sub>3</sub>Co<sub>4</sub>O<sub>9</sub>, *J. Phys. Chem. C* 119 (2015) 7979–7986, <https://doi.org/10.1021/jp512012d>.
- [7] A.C. Masset, C. Michel, A. Maignan, M. Hervieu, O. Toulemonde, F. Studer, B. Raveau, Misfit-layered cobaltite with an anisotropic giant magnetoresistance: Ca<sub>3</sub>Co<sub>4</sub>O<sub>9</sub>, *Phys. Rev. B* 62 (2000) 166–175, <https://doi.org/10.1103/PhysRevB.62.166>.
- [8] D. Kenfaui, M. Gomina, J.G. Noudem, D. Chateigner, Anisotropy of transport properties correlated to grain boundary density and quantified texture in thick oriented Ca<sub>3</sub>Co<sub>4</sub>O<sub>9</sub> ceramics, *Materials* 11 (2018) 1224, <https://doi.org/10.3390/ma11071224>.
- [9] S. Katsuyama, Y. Takiguchi, M. Ito, Synthesis of Ca<sub>3</sub>Co<sub>4</sub>O<sub>9</sub> ceramics by polymerized complex and hydrothermal hot-pressing processes and the investigation of its thermoelectric properties, *J. Mater. Sci.* 43 (2008) 3553–3559, <https://doi.org/10.1007/s10853-008-2561-x>.
- [10] N.Y. Wu, T.C. Holgate, N.V. Nong, N. Pryds, S. Linderoth, High temperature thermoelectric properties of Ca<sub>3</sub>Co<sub>4</sub>O<sub>9+δ</sub> by autocombustion synthesis and spark plasma sintering, *J. Eur. Ceram. Soc.* 34 (2014) 925–931, <https://doi.org/10.1016/j.jeurceramsoc.2013.10.022>.
- [11] A.K. Królicka, M. Piersa, A. Mirowska, M. Michalska, Effect of sol-gel and solid-state synthesis techniques on structural, morphological and thermoelectric performance of Ca<sub>3</sub>Co<sub>4</sub>O<sub>9</sub>, *Ceram. Int.* 44 (2018) 13736–13743, <https://doi.org/10.1016/j.ceramint.2018.04.215>.
- [12] S. Lin, J. Selig, Self-propagating high-temperature synthesis of Ca<sub>1.24</sub>Co<sub>1.62</sub>O<sub>3.86</sub> thermoelectric powders, *J. Alloys Compd.* 503 (2010) 402–409, <https://doi.org/10.1016/j.jallcom.2010.05.018>.
- [13] D. Kenfaui, B. Lenoir, D. Chateigner, B. Ouladid, M. Gomina, J.G. Noudem, Development of multilayer textured Ca<sub>3</sub>Co<sub>4</sub>O<sub>9</sub> materials for thermoelectric generators: influence of the anisotropy on the transport properties, *J. Eur. Ceram. Soc.* 32 (2012) 2405–2414, <https://doi.org/10.1016/j.jeurceramsoc.2012.03.022>.

- [14] S. Bresch, B. Mieller, D. Schönauer-Kamin, R. Moos, T. Reimann, F. Giovannelli, T. Rabe, Influence of pressure and dwell time on pressure-assisted sintering of calcium cobaltite, *J. Am. Ceram. Soc.* 104 (2020) 917–927, <https://doi.org/10.1111/jace.17541>.
- [15] W. Wang, Y. Liu, Y. Xue, Z. Yin, W. Lee, Z.-G. Chen, L. Yang, K. Koumoto, J. Yang, W. Li, S. Li, Separation of electric and thermal transport with *in-situ* precipitates matrix in  $\text{Ca}_3\text{Co}_4\text{O}_9$ , *Acta Mater.* 260 (2023) 119347 <https://doi.org/10.1016/j.actamat.2023.119347>.
- [16] Y. Liu, Y. Lin, Z. Shi, C.-W. Nan, Preparation of  $\text{Ca}_3\text{Co}_4\text{O}_9$  and improvement of its thermoelectric properties by spark plasma sintering, *J. Am. Ceram. Soc.* 88 (2005) 1337–1340, <https://doi.org/10.1111/j.1551-2916.2005.00284.x>.
- [17] Y. Zhang, J. Zhang, Rapid reactive synthesis and sintering of textured  $\text{Ca}_3\text{Co}_4\text{O}_9$  ceramics by spark plasma sintering, *J. Mater. Process. Technol.* 208 (2008) 70–74, <https://doi.org/10.1016/j.jmatprotec.2007.12.093>.
- [18] N. Kanas, S.P. Singh, M. Rotan, M. Saleemi, M. Bittner, A. Feldhoff, T. Norby, K. Wik, T. Grande, M.-A. Einarsson, Influence of processing on stability, microstructure and thermoelectric properties of  $\text{Ca}_3\text{Co}_{4-x}\text{O}_{9+\delta}$ , *J. Eur. Ceram. Soc.* 38 (2018) <https://doi.org/10.1016/j.jeurceramsoc.2017.11.011>, 1592–1599.
- [19] X. Li, J. Wu, S. Huang, Y. Gao, D. Liu, J. Liu, H.-T. Lin, Enhancing thermoelectric properties of  $\text{Ca}_3\text{Co}_4\text{O}_9$  ceramics through oscillatory pressure sintering, *J. Mater. Res. Technol.* 28 (2024) 3475–3484, <https://doi.org/10.1016/j.jmrt.2023.12.256>.
- [20] T. Schulz, J. Töpfer, Thermoelectric properties of  $\text{Ca}_3\text{Co}_4\text{O}_9$  ceramics prepared by an alternative pressure-less sintering/annealing method, *J. Alloys Compd.* 659 (2016) 122–126, <https://doi.org/10.1016/j.jallcom.2015.11.001>.
- [21] Z. Shi, J. Xu, J. Zhu, R. Zhang, M. Qin, Z. Lou, T. Gao, M. Reece, F. Gao, High thermoelectric performance of  $\text{Ca}_3\text{Co}_4\text{O}_9$  ceramics with duplex structure fabricated via two-step pressureless sintering, *J. Mater. Sci. Mater. Electron.* 31 (2020) 2938–2948, <https://doi.org/10.1007/s10854-019-02838-0>.
- [22] A.I. Klyndyuk, E.A. Chizhova, E.A. Tugova, R.S. Latypov, O.N. Karpov, M. V. Tomkovich, Thermoelectric multiphase ceramics based on layered calcium cobaltite, as synthesized using two-stage sintering, *Glass Phys. Chem.* 46 (2020) 562–569, <https://doi.org/10.1134/S1087659620060127>.
- [23] A.I. Klyndyuk, E.A. Chizhova, R.S. Latypov, S.V. Shevchenko, V.M. Kononovich, Effect of the addition of copper particles on the thermoelectric properties of the  $\text{Ca}_3\text{Co}_4\text{O}_{9+\delta}$  ceramics produced by two-step sintering, *Russ. J. Inorg. Chem. (Engl. Transl.)* 67 (2022) 237–244, <https://doi.org/10.1134/S0036023622020073>.
- [24] A. Chatterjee, A.E. Sachat, A. Banik, K. Biswas, A. Castro-Alvarez, C.M.S. Torres, J. Santiso, E. Chavez-Angel, Improved high temperature thermoelectric properties in misfit  $\text{Ca}_3\text{Co}_4\text{O}_9$  by thermal annealing, *Energies* 16 (2023) 5162, <https://doi.org/10.3390/en16115162>.
- [25] M. Prevel, O. Perez, J.G. Noudem, Bulk textured  $\text{Ca}_{2.5}(\text{RE})_{0.5}\text{Co}_4\text{O}_9$  (RE: Pr, Nd, Eu, Dy and Yb) thermoelectric oxides by sintering, *Solid State Sci.* 9 (2007) 231–235, <https://doi.org/10.1016/j.solidstatesciences.2007.01.003>.
- [26] A.I. Klyndyuk, I.V. Matsukevich, Synthesis and properties of  $\text{Ca}_{2.5}\text{Ln}_{0.5}\text{Co}_4\text{O}_{9+\delta}$  (Ln = La, Nd, Sm, Tb–Er), *Inorg. Mater.* 48 (2012) 1052–1057, <https://doi.org/10.1134/S0020168512090099>.
- [27] S. Li, R. Funahashi, I. Matsubara, K. Ueno, S. Sodeoka, H. Yamada, Synthesis and thermoelectric properties of the New oxide materials  $\text{Ca}_{3-x}\text{Bi}_x\text{Co}_4\text{O}_{9+\delta}$  ( $0.0 < x < 0.75$ ), *Chem. Mater.* 12 (2000) 2424–2427, <https://doi.org/10.1021/cm000132r>.
- [28] R. Tian, T. Zhang, D. Chu, R. Donelson, L. Tao, S. Li, Enhancement of high temperature thermoelectric performance in Bi, Fe co-doped layered oxide-based material  $\text{Ca}_3\text{Co}_4\text{O}_{9+\delta}$ , *J. Alloys Compd.* 615 (2014) 311–315, <https://doi.org/10.1016/j.jallcom.2014.06.190>.
- [29] I.V. Matsukevich, A.I. Klyndyuk, E.A. Tugova, A.N. Kovalenko, A.A. Marova, N. S. Krasutskaya, Thermoelectric properties of  $\text{Ca}_{3-x}\text{Bi}_x\text{Co}_4\text{O}_{9+\delta}$  ( $0.0 \leq x \leq 1.5$ ) ceramics, *Inorg. Mater.* 52 (2016) 593–599, <https://doi.org/10.1134/S0020168516060091>.
- [30] T. Liu, D. Bao, Y. Wang, H. Gao, D. Zhou, G. Han, J. Tang, Z.-Y. Huang, L. Yang, Z.-G. Chen, Exploring thermoelectric performance of  $\text{Ca}_3\text{Co}_4\text{O}_{9+\delta}$  ceramics via chemical electrodeless plating with Cu, *J. Alloys Compd.* 821 (2020) 153522, <https://doi.org/10.1016/j.jallcom.2019.153522>.
- [31] S. Punitsontorn, N. Lersongkram, A. Harnwungmoung, K. Kurosaki, S. Yamanaka, Synthesis, mechanical and magnetic properties of transition metals-doped  $\text{Ca}_3\text{Co}_{3.8}\text{M}_{0.2}\text{O}_9$ , *J. Alloys Compd.* 503 (2010) 431–435, <https://doi.org/10.1016/j.jallcom.2010.05.027>.
- [32] S. Demirel, E. Altin, E. Oz, S. Altin, A. Bayri, An enhancement ZT and spin state transition of  $\text{Ca}_3\text{Co}_4\text{O}_9$  with Pb doping, *J. Alloys Compd.* 627 (2015) 430–437, <https://doi.org/10.1016/j.jallcom.2014.11.200>.
- [33] A.I. Klyndyuk, I.V. Matsukevich, Synthesis, structure, and properties of  $\text{Ca}_3\text{Co}_{3.85}\text{M}_{0.15}\text{O}_{9+\delta}$  (M = Ti–Zn, Mo, W, Pb, Bi) layered thermoelectrics, *Inorg. Mater.* 51 (2015) 944–950, <https://doi.org/10.1134/S0020168515080105>.
- [34] Y.-n. Li, P. Wu, S. Zhang, X. Han, S. Chen, L. Wang, Enhanced  $\text{Ca}_3\text{Co}_4\text{O}_9$  thermoelectric transport properties through Gd doping based on spin entropy and size effect, *J. Alloys Compd.* 973 (2024) 172904, <https://doi.org/10.1016/j.jallcom.2023.172904>.
- [35] S. Neelakandan, K. Biswas, Tweaking the interplay of the layers by substitution in  $\text{Ca}_3\text{Co}_4\text{O}_{9+\delta}$  for high efficiency thermoelectric materials, *J. Alloys Compd.* 971 (2024) 172693, <https://doi.org/10.1016/j.jallcom.2023.172693>.
- [36] A. Soffientini, P. Chigna, G. Spinolo, S. Boldrini, A. Famengo, U.A. Tamburini, Nanostructured calcium cobalt oxide  $\text{Ca}_3\text{Co}_4\text{O}_9$  as thermoelectric material. Effect of nanostructure on local coordination, Co charge state and thermoelectric properties, *J. Phys. Chem. Solid.* 143 (2020) 109474, <https://doi.org/10.1016/j.jpcs.2020.109474>.
- [37] N. Puri, R.P. Tandon, M.V.G. Padmavati, A.K. Mahapatro, Defect states in graphene oxide mixed nanostructured calcium cobalt oxide, *J. Alloys Compd.* 963 (2020) 171232, <https://doi.org/10.1016/j.jallcom.2023.171232>.
- [38] P. Carvillo, Y. Chen, C. Boyle, P.N. Barnes, X. Song, Thermoelectric performance enhancement of calcium cobaltite through barium grain boundary segregation, *Inorg. Chem.* 54 (2015) 9027–9032, <https://doi.org/10.1021/acs.inorgchem.5b01296>.
- [39] P.-H. Xiang, Y. Kinemuchi, H. Kaga, K. Watari, Fabrication and thermoelectric properties of  $\text{Ca}_3\text{Co}_4\text{O}_9/\text{Ag}$  composites, *J. Alloys Compd.* 454 (2008) 364–369, <https://doi.org/10.1016/j.jallcom.2006.12.102>.
- [40] Y. Wang, Y. Sui, J. Cheng, X. Wang, W. Su, Comparison of the high temperature thermoelectric properties for Ag-doped and Ag-added  $\text{Ca}_3\text{Co}_4\text{O}_9$ , *J. Alloys Compd.* 477 (2009) 817–821, <https://doi.org/10.1016/j.jallcom.2008.10.162>.
- [41] F. Kahraman, M.A. Madre, Sh Rasekh, C. Salvador, P. Bosque, M.A. Torres, J. C. Diez, A. Sotelo, Enhancement of mechanical and thermoelectric properties of  $\text{Ca}_3\text{Co}_4\text{O}_9$  by Ag addition, *J. Eur. Ceram. Soc.* 35 (2015) 3835–3841, <https://doi.org/10.1016/j.jeurcermsoc.2015.05.029>.
- [42] F. Delorme, P. Diaz-Chao, E. Guilmeau, F. Giovannelli, Thermoelectric properties of  $\text{Ca}_3\text{Co}_4\text{O}_9$ - $\text{Co}_3\text{O}_4$  composites, *Ceram. Int.* 41 (2015) 10038–10043, <https://doi.org/10.1016/j.ceramint.2015.04.091>.
- [43] R.K. Gupta, R. Sharma, A.K. Mahapatro, R.P. Tandon, The effect of  $\text{ZrO}_2$  dispersion on the thermoelectric power factor of  $\text{Ca}_3\text{Co}_4\text{O}_9$ , *Physica B* 483 (2016) 48–53, <https://doi.org/10.1016/j.physb.2015.12.028>.
- [44] O. Jankovsky, S. Huber, D. Sedmidubský, L. Nádherný, T. Hlásek, Z. Sofer, Towards highly efficient thermoelectrics:  $\text{Ca}_3\text{Co}_4\text{O}_{9+\delta}$ - $n\text{CaZrO}_3$  composite, *Ceramics* 58 (2014) 106–110.
- [45] I.V. Matsukevich, A.I. Klyndyuk, E.A. Tugova, M.V. Tomkovich, N.S. Krasutskaya, V.V. Gusarov, Synthesis and properties of materials based on layered calcium and bismuth cobaltites, *Russ. J. Appl. Chem.* 88 (2015) 1241–1247, <https://doi.org/10.1134/S1070427215080030>.
- [46] C. Ruan, H. Song, M. Fan, H. Hao, S. Liu, Enhancement of  $\text{Ca}_3\text{Co}_4\text{O}_{9+\delta}$  thermoelectric properties by dispersing SiC nanoparticles, *Ceram. Int.* 47 (2021) 6548–6553, <https://doi.org/10.1016/j.ceramint.2020.10.242>.
- [47] H. Amaveda, M. Mora, O.J. Dura, M.A. Torres, M.A. Madre, S. Marinel, A. Sotelo, Drastic enhancement of mechanical properties of  $\text{Ca}_3\text{Co}_4\text{O}_9$  by  $\text{B}_4\text{C}$  addition, *J. Eur. Ceram. Soc.* 41 (2021) 402–408, <https://doi.org/10.1016/j.jeurceramsoc.2020.08.024>.
- [48] X.-D. Zhou, L.R. Pederson, E. Thomsen, Z. Nie, G. Coffey, Nonstoichiometry and transport properties of  $\text{Ca}_3\text{Co}_{4-x}\text{O}_{9+\delta}$ , *Electrochem. Solid State Lett.* 12 (2009) F1–F3, <https://doi.org/10.1149/1.3039948>.
- [49] M. Tahashi, K. Ogawa, M. Takahashi, H. Goto, Effect of compositional ratio of cobalt to calcium on crystal phase and thermoelectric properties of oxide thermoelectric material composed of sintered  $\text{Ca}_3\text{Co}_4\text{O}_9/\text{Ca}_3\text{Co}_2\text{O}_6$  mixture, *J. Ceram. Soc. Jpn.* 121 (2013) 444–447.
- [50] H. Amaveda, O.J. Dura, M. Mora, M.A. Torres, G. Guelou, M.A. Madre, S. Marinel, A. Sotelo, Tuning  $\text{Ca}_3\text{Co}_4\text{O}_9$  thermal and transport properties by TiC nanoparticles addition, *Bol. Soc. Esp. Ceram. Vidr.* 60 (2021) 138–146, <https://doi.org/10.1016/j.jbsecv.2020.03.006>.
- [51] J.-n. Li, P. Wu, S. Zhang, Y. Pei, J. Yang, S. Chen, L. Wang, Enhanced thermoelectric properties of  $\text{Ca}_3\text{Co}_4\text{O}_9$  by adding nano  $\text{MoSi}_2$ , *Ceram. Int.* 48 (2022) 33967–33975, <https://doi.org/10.1016/j.ceramint.2022.07.346>.
- [52] D. Sedmidubský, V. Jakeš, O. Jankovský, J. Leitner, Z. Sofer, J. Hejtmánek, Phase equilibria in Ca–Co–O system, *J. Solid State Chem.* 194 (2012) 199–205, <https://doi.org/10.1016/j.jssc.2012.05.014>.
- [53] A.I. Klyndyuk, I.V. Matsukevich, M. Janek, E.A. Chizhova, Z. Lenčes, O. Hanzel, P. Veteška, Thermoelectric properties of a phase-heterogeneous ceramic based on  $\text{Ca}_3\text{Co}_4\text{O}_{9+\delta}$  prepared by hot pressing, *Russ. J. Appl. Chem.* 93 (2020) 1126–1131, <https://doi.org/10.1134/S1070427220080030>.
- [54] A.I. Klyndyuk, G.S. Petrov, A.F. Polyuan, L.A. Bashkirov, Structure and physicochemical properties of  $\text{Y}_2\text{Ba}_{1-x}\text{M}_x\text{CuO}_5$  (M = Sr, Ca) solid solutions, *Inorg. Mater.* 35 (1999) 512–516.
- [55] A.I. Klyndyuk, N.S. Krasutskaya, A.A. Khort, Synthesis and properties of ceramics based on a layered bismuth calcium cobaltite, *Inorg. Mater.* 54 (2018) 509–514, <https://doi.org/10.1134/S0020168518050059>.
- [56] D. Lu, G. Chen, J. Pei, X. Yang, H. Xian, Effect of erbium substitution on thermoelectric properties of complex oxide  $\text{Ca}_3\text{Co}_2\text{O}_6$  at high temperatures, *J. Rare Earths* 26 (2008) 168–172, [https://doi.org/10.1016/S1002-0721\(08\)60059-9](https://doi.org/10.1016/S1002-0721(08)60059-9).
- [57] K. Park, D.A. Hakeem, J.S. Cha, Synthesis and structural properties of thermoelectric  $\text{Ca}_{3-x}\text{Ag}_x\text{Co}_4\text{O}_{9+\delta}$  powders, *Dalton Trans.* 45 (2016) 6990–6997, <https://doi.org/10.1039/C5DT04959H>.
- [58] C.S. Lim, C.K. Chua, Z. Sofer, O. Jankovský, M. Pumera, Alternating misfit layered transition/alkaline earth metal chalcogenide  $\text{Ca}_3\text{Co}_4\text{O}_9$  as a New class of chalcogenide materials for hydrogen evolution, *Chem. Mater.* 26 (2014) 4130–4136, <https://doi.org/10.1021/cm501181j>.
- [59] S. Yu, S. He, H. hen, L. Guo, Effect of calcination temperature on oxidation state of cobalt in calcium cobaltite and relevant performance as intermediate-temperature solid oxide fuel cell cathodes, *J. Power Sources* 280 (2015) 581–587, <https://doi.org/10.1016/j.jpowsour.2015.01.150>.
- [60] Y. Huang, B. Zhao, R. Ang, S. Lin, Z. Huang, S. Tan, Y. Li, W. Song, Y. Sun, Enhanced thermoelectric performance and room-temperature spin-state transition of  $\text{Co}^{4+}$  ions in the  $\text{Ca}_3\text{Co}_{4-x}\text{Rh}_x\text{O}_9$  system, *J. Phys. Chem. C* 117 (2013) 11459–11470, <https://doi.org/10.1021/jp400146y>.
- [61] M.A. Mohammed, M.B. Uday, S. Izman, Enhanced thermoelectric performance of  $\text{Ca}_3\text{Co}_4\text{O}_9$  doped with aluminum, *J. Mater. Sci. Mater. Electron.* 31 (2020) 16569–16582, <https://doi.org/10.1007/s10854-020-04212-x>.
- [62] Y.-H. Lin, J. Lan, Z. Shen, Y. Liu, C.-W. Nan, J.-F. Li, High-temperature electrical transport behaviors in textured  $\text{Ca}_3\text{Co}_4\text{O}_9$ -based polycrystalline ceramics, *Appl. Phys. Lett.* 94 (2009) 072107, <https://doi.org/10.1063/1.3086875>.

- [63] J. Yu, K. Chen, F. Azough, D.T. Alvarez-Ruiz, M.I. Reece, R. Freer, Enhancing the thermoelectric performance of calcium cobaltite ceramics by tuning composition and processing, *ACS Appl. Mater. Interfaces* 12 (2020) 47634–47646, <https://doi.org/10.1021/acsami.0c14916>.
- [64] S. Raghavan, M.J. Mayo, H. Wang, R.B. Dinwiddie, W.D. Porter, The effect of grain size, porosity and yttria content on the thermal conductivity of nanocrystalline zirconia, *Scripta Mater.* 39 (1998) 1119–1125, [https://doi.org/10.1016/S1359-6462\(98\)00290-5](https://doi.org/10.1016/S1359-6462(98)00290-5).
- [65] L. Wu, Q. Meng, C. Jooss, J.-C. Zheng, H. Inada, D. Su, Q. Li, Y. Zhu, Origin of phono glass-electron crystal behavior in thermoelectric layered cobaltate, *Adv. Funct. Mater.* 23 (2013) 5728–5736, <https://doi.org/10.1002/adfm.201301098>.